High-Temperature-Induced Pore System Evolution of Immature Shale with Different Total Organic Carbon Contents

Luo Zhuoke, Tiefeng Lin, Xin Liu, Shengming Ma, Xin Li, Fan Yang, Bo He, Jun Liu, Yao Zhang, and Lingzhi Xie*

Read Online

ACCESS | Metrics & More | Article Recommendations

ABSTRACT: The pyrolysis process of source rock, especially organic-rich immature shale, is required for oil and gas extraction, during which the evolution of the pore structure system in the immature shale determines the heat conduction and fluid flow under the heating treatment. Although some sound achievements have been made regarding the pyrolysis of immature shale, the effect of the total organic carbon (TOC) content on the pore structure evolution of immature shale remains unclear. With respect to this issue, in this work, a series of N_2 adsorption/desorption and nuclear magnetic resonance (NMR) experiments were conducted, and fractal dimension theory was also introduced to analyze the pore structure evolution of immature shale subjected to heating treatment in a quantitative manner. The results indicate

that the adsorption branch of the nitrogen adsorption−desorption isotherm can be divided into three stages. The pore structure of different TOC immature shales does not change significantly, and they are all slit-shaped. In addition, immature shale with a higher organic content has a higher hydrocarbon expulsion strength and a higher pore volume growth rate, which indicate that the pyrolysis of organic matter greatly affects the pore structure of immature shale during heating. This phenomenon shows that the pyrolysis of organic matter greatly influences the pore structure of immature shale during the heating process. The pores of immature shale in the study area have significant fractal characteristics, the fractal dimension is between 2.397 and 2.636, the pore space of the sample is extremely small, the pore structure is extremely complex, and the heterogeneity is strong.
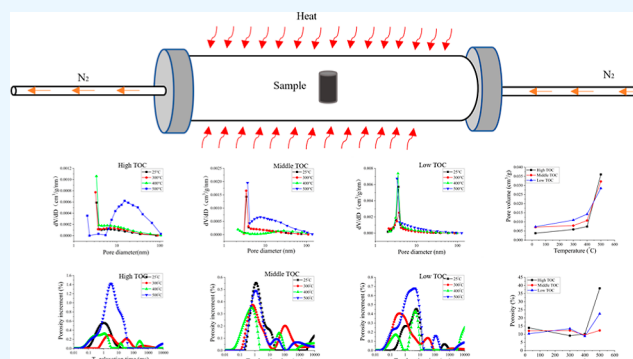
1. INTRODUCTION

Unconventional oil and gas resources have been recognized as an important alternative energy source for petroleum energy.[1,2] Immature shale is a kind of sedimentary rock with inorganic minerals and solid organic matter, mainly kerogen and a small amount of asphaltene.[3−5] At present, the exploitation of immature shale is mainly based on surface dry distillation. However, due to high costs, a high mining intensity, a slow development and utilization rate, environmental pollution, and other reasons, the surface dry distillation method has not yet been developed on a large scale.[6−9] The research focus has been shifted to the underground dry distillation technology of immature shale. The essence of immature shale development and utilization is to heat solid organic matter to pyrolysis temperatures and degrade it into oil and gas resources.[10] The pyrolysis of kerogen causes a large number of pores and cracks in the solid skeleton of immature shale.[11,12] The formation of new pores and fractures provides a channel for the heating of immature shale and also for the flow of oil and gas generated by pyrolysis.[13−15] Therefore, the accurate characterization of pore structure and the accurate understanding of thermal evolution

mechanisms in the process of in situ production of immature shale is of great significance to analyze the seepage and production processes of pyrolysis-derived oil and gas and to guide the in situ development technology of immature shale.[16−18]

To date, encouraging investigations have been performed to capture the pore structures of post-pyrolysis immature shale samples. Rabbani et al.[19] and Saif et al.[20] used CT equipment to study the pore characteristics of Green River shale before and after pyrolysis, and the results demonstrated that the porosity and crack aperture critically increased in the temperature range of 380 to 400 °C. Sun et al.[21] and Han et al.[22] found that kerogen would first be converted into asphalt during pyrolysis by low-temperature nitrogen adsorption/desorption (LTNA), and
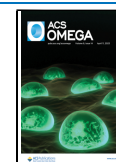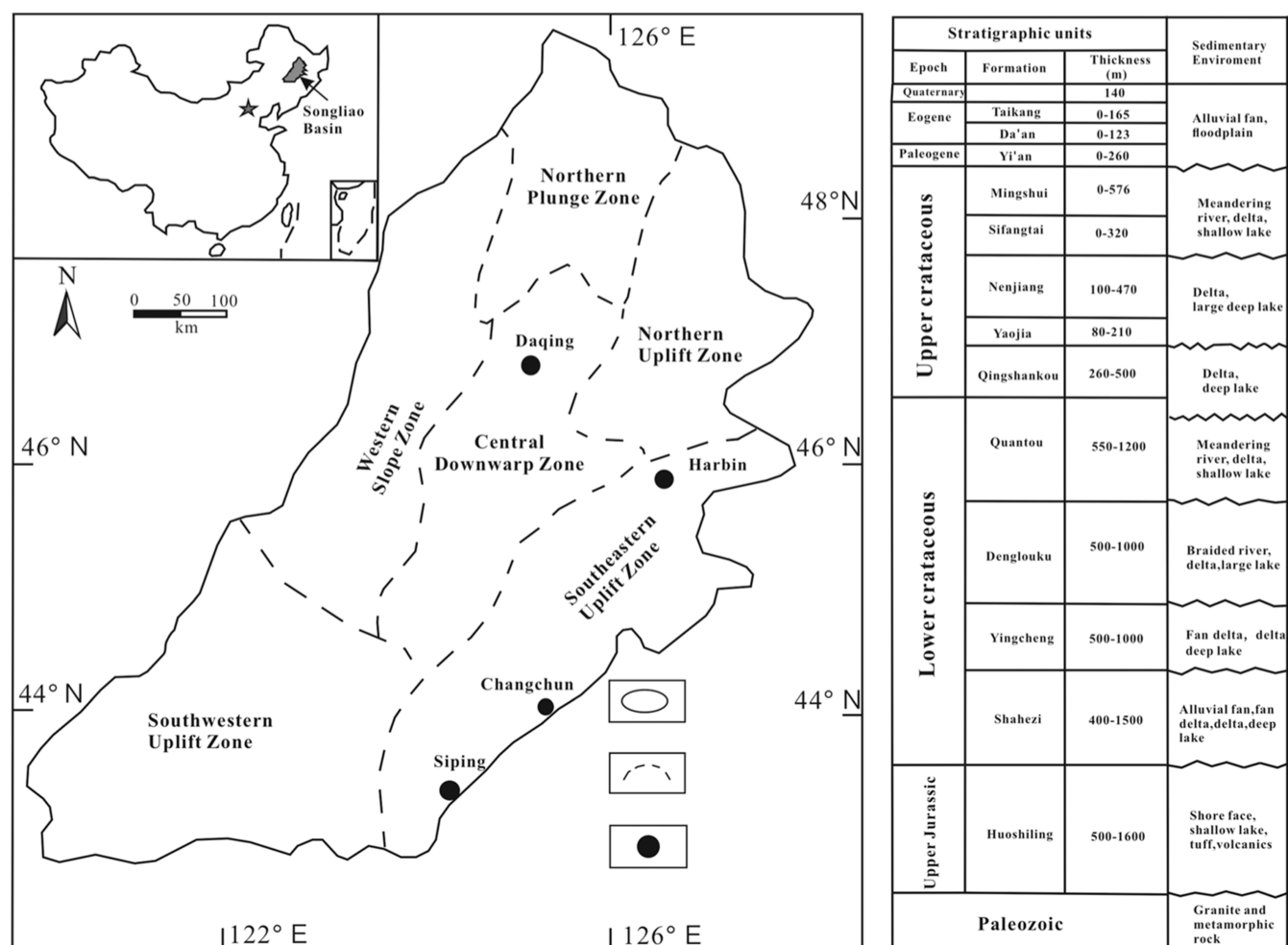
Figure 1. Structural units with locations relevant to the pilot project.[28]

asphalt would lead to pore plugging, reducing the pore volume and specific surface area. Yang et al.[23] studied the pore size evolution characteristics of shale after heat treatment at different temperatures by the mercury injection capillary pressure (MICP), indicating that the pore volume, average pore size and porosity of oil shale increased significantly with increasing temperature. Bai et al.[24] studied the internal pore structure of shale in the pyrolyzed process in the range of 100−800 °C by scanning electron microscopy and LTNA methods, indicating that in the temperature range of 350−450 °C, there is a linear relationship between the fractal dimension and the average pore size. Geng et al.[25] studied the evolution characteristics of the internal pore structure of immature shale under different pressure and temperature conditions, indicating that the coupling effect of temperature and pressure aggravates the degree of pyrolysis and fracturing of the immature shale and jointly promotes the generation of pores and fractures.

In the past, the study of immature shale mainly focused on the influence of temperature and pressure on the evolution of the pore structure of immature shale. Some scholars have also studied the effect of organic matter pyrolysis on the pore structure of immature shale. Tisot[26] conducted an experimental study on the change in pore morphology in Green River shale with different organic matter contents after heating, indicating that the organic matter content was directly related to the newly formed fractures and pore volume. Tiwari et al.[18] used CT to study the change in the pore structure after pyrolysis of shale in

the temperature range of 350−500 °C, and the results show that its pore structure mainly depends on the distribution state of kerogen. Kobchenko et al.[27] and Saif et al.[20] demonstrated that the thermal action on organic-rich rocks at temperatures close to 350 °C could lead to the formation of single cracks in the sample, which were formed by the overpressure when the kerogen was converted into hydrocarbon. Basically, there have been considerable studies on the influence of organic matter pyrolysis on the pore structure in immature shale, while research on the pore structure evolution mechanism of immature shale with different organic contents after pyrolysis is relatively weak. Actually, in the process of in situ mining, the TOC content of immature shale in different layers varies greatly; therefore, the evolution law of the pore structure of immature shale with different TOC contents should be considered.

This paper takes the immature shale of the Qingshankou Formation in the Songliao Basin, Northeast China, as the research object. Combined with the N$_2$ adsorption/desorption method and NMR experiments, the pore structures of immature shale specimens with variable TOC contents were analyzed before and after pyrolysis. The fractal method was used to analyze the evolution of the pore structure before and after pyrolysis of immature shale with different TOC contents from a microscopic point of view.

2. GEOLOGICAL SETTING

As shown in Figure 1, the Songliao Basin is located in Northeast China and spans the three provinces of Heilongjiang, Jilin, and Liaoning. The basin is shaped like a rhombus and extends from northeast to southwest, the west is bound by the Nenjiang fault, and the east is bound by the Mudanjiang fault. The basin is 820 km long in the north-south direction and 350 km wide in the east−west direction and covers an area of approximately 26×10^4 km². The Songliao Basin is one of the most important petroleum-bearing basins in China. It is home to two major oil fields in China bound by the Nenjiang-Songhua River, with the Daqing Oilfield in the north and the Jilin Oilfield in the south.[29] The total oil resources in the middle and shallow layers in the northern part of the basin can reach 10.2 billion tons.[30] The immature shale resources in this area are mainly distributed in the northeast uplift, central depression, and southeast uplift belt.[31,32] It is a typical large-scale Mesozoic and Cenozoic continental sedimentary basin. The Songliao Basin is one of the largest Cretaceous intracratonic sedimentary rift basins on Earth and can be divided into six first-order tectonic units. The thickness of the Qingshankou Formation is 260−500 m, and the lithology is dark gray and black mudstone with immature shale and gray sandstone and siltstone.

2.1. Sampling. The source rock core samples used in the experiment were taken from the Qingshankou Formation in the Songliao Basin, Daqing. Taking 3 and 7% TOC as the thresholds for classifying low, medium, and high organic matter contents, the TOC contents of the immature shale cores were 10.5% (high organic matter content), 6.2% (medium organic matter content), and 2% (low organic matter content), respectively. To prevent weathering and deterioration from exposure to air, the samples were sealed and transported to the laboratory after on-site sampling, and the immature shale was processed into cylindrical specimens of $\varphi 5 \times 10$ mm with a wire cutting machine for NMR experimentation, as shown in Figure 2. The color of the immature shale was dark brown. The immature shale was processed into powder with a particle size of 60−80 mesh[33] for low-temperature liquid nitrogen experiments, as shown in Figure 3.
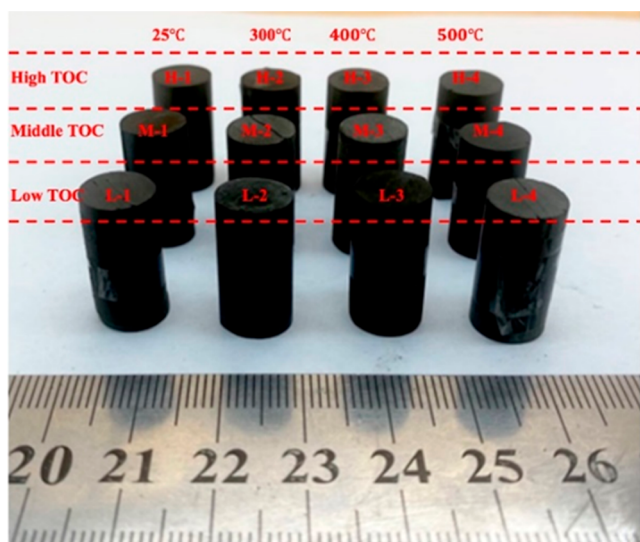

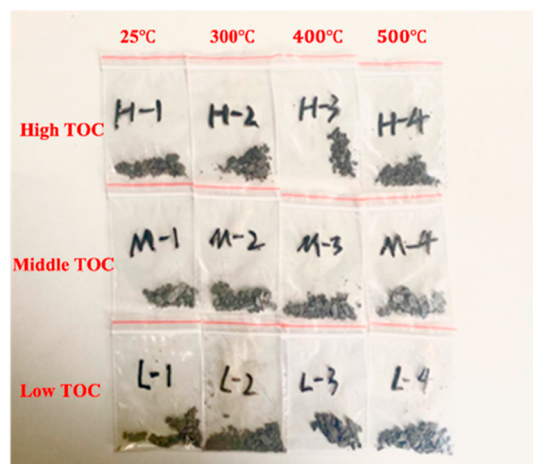**Figure 2.** Specimens for the NMR test.

Figure 3. Shale powder for N₂ adsorption/desorption experiments.

3. MATERIALS AND METHODOLOGY

3.1. Analytical Equipment and Methods. Since the kerogen contained in the immature shale starts to undergo a thermal decomposition reaction once the temperature exceeds 300 °C,[18] the temperature targets of the experiment are set to 300, 400, and 500 °C, and the normal temperature of rock is 25 °C. The samples were pyrolyzed in an OTL 1200 tube furnace. To ensure that the rock samples were evenly heated and were not affected by thermal impact stress, the heating rate was set to 2 °C/min, and the samples were heated to the target temperature in batches according to the set gradient. After holding for 2 h, the furnace was opened for natural cooling to normal temperature. After the test was finished, the samples were removed for NMR testing and isothermal adsorption/desorption analysis of low-temperature nitrogen.

The mineral composition of the sample was determined by using a TTR III multifunctional X-ray diffractometer (manufactured by Rigaku Corporation, Japan) (Table 1). Quartz and clay are the primary mineral components of the immature shale, followed by plagioclase, pyrite, and K-feldspar. The clay content of immature shale is positively correlated with TOC content, and the clay content of high-TOC immature shale is the highest, which is 70.4%. The content of ankerite in low-TOC immature shale is very high, which is 42%, while high-TOC and medium-TOC immature shale do not contain ankerite.

The low-temperature N₂ isotherm adsorption/desorption analysis was performed with a Micromeritics Instrument 2460 from the American Mike Instrument Company. Each test sample was approximately 0.1 g, and N₂ was used as the carrier gas and purged at 105 °C for 24 h. The N₂ isothermal adsorption/desorption curve was obtained by changing the pressure; the specific surface area of the sample was calculated according to the BET multilayer adsorption formula,[34] and the pore volume and pore size distribution were calculated using the BJH model.[35]

The GeoSpec2/150 NMR core analysis system of Oxford Instruments, UK, was used for NMR testing, with a frequency range of 10 kHz to 32.5 MHz and frequency resolution of 0.008 Hz; each scan can reach 12800 CPMG echoes. Before a T₂ spectrum NMR test, the rock sample was vacuumed at room temperature for 24 h, and then, the sample was placed in the vacuum saturation device for 24 h to achieve 100% water saturation. The reason for the saturation process is that ¹H NMR spectroscopy is quite effective for detecting the internal structure

Table 1. Mineral Components of the TOC High-, Medium-, and Low-TOC Immature Shale

sample type	mineral composition (%)							
	quartz	K-feldspar	plagioclase	calcite	siderite	pyrite	ankerite	clay
high-TOC immature shale	17.4	1.7	5.8	2.0		2.5		70.4
medium-TOC immature shale	18.2	0.9	5.1	29.7	3.1	3.1		39.9
low-TOC immature shale	15.3	1.5	3.6	2.5		8.7	42	26.4

of porous materials.[36] During the measurement of dynamic processes via NMR spectroscopy, the CPMG pulse sequence was utilized to generate the T_2 spectrum (or T_2 distribution), which can indicate the pore size distribution of the tested samples.

3.2. Fractal Theory. The methods for calculating the fractal dimension of nanoscale pores from low-temperature liquid nitrogen adsorption data mainly include the fractal BET model,[37] fractal FHH model, and thermodynamic model,[38] among which the fractal FHH model is the most widely used, and its calculation method is mainly based on the following formula[39]

$$C + A\left[\ln\left(\frac{P_0}{P}\right)\right] \tag{1}$$

where V—the amount of gas adsorbed under equilibrium pressure, cm^3·g^{-1}; V_m—volume of adsorbed gas in a monolayer, P_0—saturation pressure of gas adsorption, Pa; P—equilibrium pressure, Pa; C—adsorption heat constant; and A—ln V and the logarithmic slope of the $\ln(\ln P_0/P)$ curve, controlled by the fractal dimension D and the adsorption mechanism. Regarding the specific calculation of the fractal dimension, according to the different adsorption mechanisms of the gas, two commonly used algorithms have been used. One considers that the adsorption of the gas to the medium is controlled by the van der Waals force of the molecules between the interfaces. At this time, the fractal dimension can be expressed as

$$D = 3A + 3 \tag{2}$$

Another consideration is that the force between the medium and the gas mainly comes from the effect of surface tension, and the fractal dimension based on this can be expressed as

$$D = A + 3 \tag{3}$$

The abovementioned calculation may make the fractal dimension larger than 3 or smaller than 2, thus losing its fractal significance. In the nitrogen adsorption process, the adsorption on the interface under the relative pressure is often the result of the combined action of two forces: in the initial stage of adsorption, the gas molecules are adsorbed in a single layer, and the van der Waals force plays a controlling role at this time; as the relative pressure increases, if the gas content is high, the gas changes from single-layer adsorption to multilayer adsorption, resulting in capillary condensation. At this time, the effect of surface tension is prominent, and the surface van der Waals force is negligible. The adsorption of gas by immature shale is often due to a combination of van der Waals forces and surface tension. In the calculation performed in this paper, the parameter δ introduced by Ismail and Pfeifer[40] is used

$$\delta = 3(1 + A) - 2 \tag{4}$$

According to the research results of Yao et al.,[41] when the relative pressure is 0.5–1, the fractal dimension reflects the complexity of the pore structure, and when the relative pressure is 0–0.5, the fractal dimension reflects the complexity of the pore surface. Therefore, in this paper, the fractal dimension D_{FHH} of the pore structure and the fractal dimension D_S of the pore surface are calculated by piecewise fitting nitrogen adsorption data. According to formula 1, A can be obtained by linear fitting of the double logarithmic curve. Formula 3 is used to calculate the fractal dimension.

4. RESULTS AND DISCUSSION

4.1. N$_2$ Adsorption/Desorption Test. *4.1.1. Pore Structure Type.* The adsorption of different materials and their pore distributions control the shape of the adsorption isotherm, and the surface properties of the material can be analyzed according to the type of adsorption curve.[42,43] The isothermal curves of immature shale at different pyrolysis temperatures are shown in Figure 4.

The adsorption branch of the nitrogen adsorption–desorption isotherm can be divided into three stages, under the lower relative pressure ($P/P_0 < 0.4$), the adsorption isotherm rises slowly and presents a gentle convex shape. This stage corresponds to the monolayer adsorption of liquid nitrogen on the sample surface,[44] and at moderate pressure ($P/P_0 = 0.4$–0.8), the adsorption branch rises stably and a hysteresis ring appears, indicating the existence of a large mesoporous network, which corresponds to the multilayer adsorption stage.[45] At higher pressures ($P/P_0 = 0.8$–1.0), the adsorption branches rise sharply, and even when P/P_0 is close to 1.0, the adsorption branches do not show the platform, thus indicating that the sample has a heterogeneous pore structure containing a wide pore size from micropores to mesopores.[42,46] The isothermal desorption curve of the experimental sample showed obvious desorption hysteresis, the amount of desorption was much smaller than the adsorption amount, and there was a significant hysteresis loop because the pore structure of the sample was extremely complex, and capillary condensation occurred on the surface of the matrix,[47] reflecting that there were significant differences in the development morphology and connectivity of the pores of the small pore size of the sample, resulting in the incomplete desorption of the adsorbed nitrogen. The degree of hysteresis loop development was different in each sample, but the overall morphology was basically similar, which was closest to the H3 type in the IUPAC hysteresis ring classification,[48] indicating that the pores were slit type, indicating that the sample had more flaky granular matrix, which was consistent with the clay minerals containing a higher mass fraction in immature shale. After pyrolysis at different temperatures, the pore structure of different TOC immature shale does not change significantly, and they are all slit-shaped.

4.1.2. Pore Size Distribution. According to the IUPAC classification method,[49] the pore structure is divided into 3 categories according to the diameter Φ of the pores: micropores (<2 nm), mesopores (2–50 nm), and macropores (>50 nm).

The total pore volume, specific surface area, average pore diameter, and other pore characteristic parameters of immature shale specimens can be obtained by the N$_2$ adsorption/desorption method. Through the analysis and comparison of
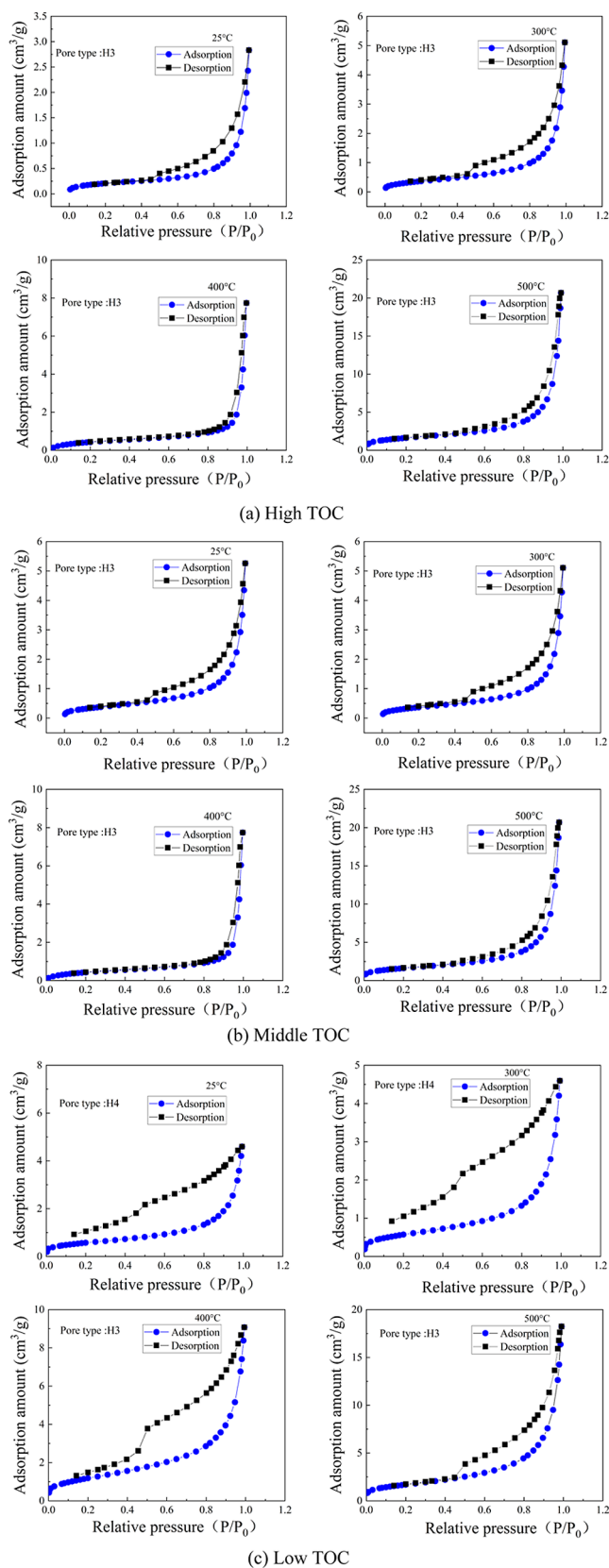
Figure 4. Adsorption desorption curves of immature shale with different TOC contents at different temperatures.

parameter values at different temperatures, the evolution characteristics of the pore structure in the immature shale can be obtained. Figure 5a−c shows the pore size distribution curves

of immature shale with high-, medium-, and low-TOC contents after pyrolysis at different temperatures. The test data are shown in Table 1. Analysis shows that these pore size distribution curves change regularly with temperature. At 25−400 °C, the pore size distribution curves of different TOC immature shale showed unimodal distribution, and the peak position of pore size did not change much, all between 2 and 3.8 nm, indicating that the pores of this size were well developed. The pore size peak of high-TOC immature shale increased with the increase of temperature, indicating that the pyrolysis of organic matter promoted the development of mesopores. At 500 °C, the pore size distribution of high- and medium-TOC immature shale is converted into a bimodal distribution, in which the peak value at 3 nm of high-TOC immature shale decreases, and the peak occurs at 15.2 nm, indicating that with the increase in temperature, the macropores begin to develop, and the average pore size increases. The pore size distribution curve of low-TOC immature shale shows a single peak distribution in the whole temperature range, indicating that the pore structure distribution is single.

The increment of nitrogen adsorption capacity of oil shale under different temperatures changes regularly (see Table 2). At 25,300 °C, the nitrogen adsorption capacity of high-TOC immature shale is lower than that of medium- and low-TOC immature shale. The nitrogen adsorption capacity of medium- and low-TOC oil shale changes significantly above 300° C. The nitrogen adsorption capacity of high-, medium-, and low-TOC immature shale in the temperature range of 300−500 °C continues to increase, among which the adsorption capacity of high-TOC oil shale at 500 °C is the largest, and the adsorption capacity is 23.588 $cm^3 \cdot g^{-1}$. As shown in Figures 6 and 7, with increasing temperature under the action of different pyrolysis temperatures, the pore volume and specific surface area of immature shale change regularly. As the temperature increases, the pore volume and specific surface area of high-TOC immature shale increase. From room temperature to the final temperature of 500 °C, the pore volume and specific surface area of high-TOC immature shale increase by 9.55 and 8.47 times, respectively. This is because in high-TOC immature shale, under the action of high temperature, organic matter cracks to form pore space, and the pressure of gas products also plays the role of "expansion".[50] The overall change trend of middle-TOC immature shale is similar to that of high-TOC immature shale, with pore volume and specific surface area increasing by 4.08 and 4.53 times, respectively, while those of low-TOC immature shale increase by 2.31 times and 1.56 times. This suggests that the higher the organic matter content of the immature shale at high temperatures, the greater the pore space and gas pressure generated by organic matter cracking, and thus, the greater the change in pore volume and specific surface area. Before 400 °C, the pore volume of the three samples from high to low is the low-TOC sample, medium-TOC sample, and high-TOC sample; this is because before 400 °C, organic matter cracking will form asphaltene, and asphaltene will block part of the pores,[51,52] and at 500 °C, because the secondary cracking of asphaltene will produce a large amount of oil and gas, the blocked pores are dredged;[53,54] hence, the pore volume of the three samples from high to low is the high-TOC sample, medium-TOC sample, low-TOC sample.

According to the classification method of the pore structure, the pore structures of the specimens with different testing temperatures and TOC contents obtained by the N_2 adsorption/desorption method were classified. The pore
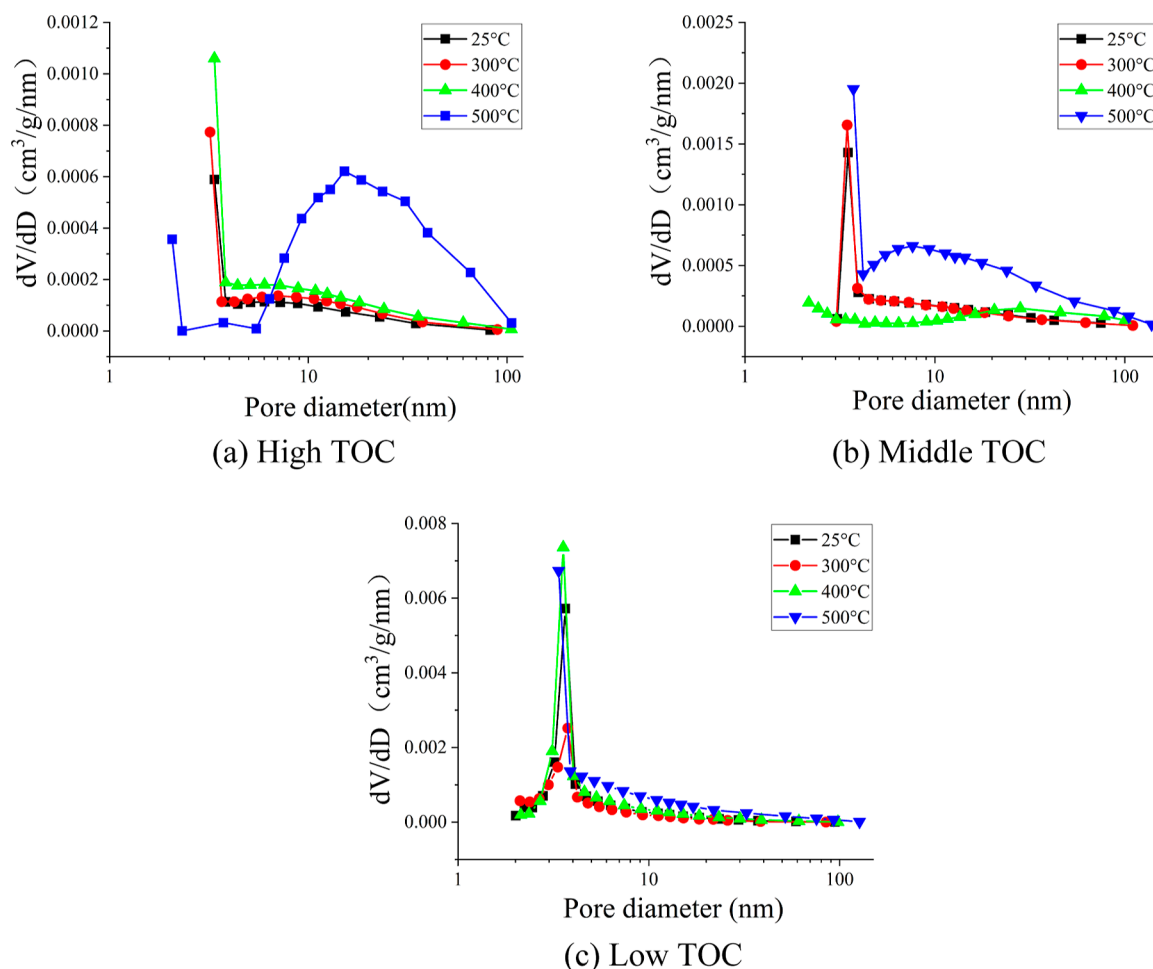
(a) High TOC

(b) Middle TOC

(c) Low TOC

Figure 5. Pore size distribution curves.

Table 2. Summary of Experimental Data

specimen number	temperature/°C	TOC content (%)	aperture peak/nm	total pore volume/ 10^{-3} cm^3·g^{-1}	N$_2$ adsorption capacity/cm^3·g^{-1}
H-1	25	10.5	3.371	3.771	2.833
M-1		6.2	3.491	7.096	5.261
L-1		2	3.654	7.321	4.595
H-2	300	10.5	3.200	5.824	3.756
M-2		6.2	3.455	7.936	5.108
L-2		2	3.763	10.970	6.949
H-3	400	10.5	3.368	7.434	4.790
M-3		6.2	2.168	10.738	7.740
L-3		2	3.562	14.234	9.074
H-4	500	10.5	15.195	35.988	23.588
M-4		6.2	3.723	32.138	20.687
L-4		2	3.372	28.375	18.236

structure histogram is shown in Figure 8, for each temperature, from left to right, the results of high-, medium-, and low-TOC immature shale at the corresponding temperature were obtained. The total pore volume of high- and medium-TOC immature shale increases with increasing temperature, and the total pore volume with the largest value is 35.99×10^{-3} cm^3·g^{-1} of that of high-TOC immature shale at 500 °C. At 25 °C, the total pore volume of high-TOC immature shale is small, and the total pore volume of high-TOC immature shale is

3.77×10^{-3} cm^3·g^{-1}. At 25−300 °C, the mesopores of high- and medium-TOC immature shale increase, which is caused by free water volatilization and dehydration of some minerals; at 300−400 °C, the volume of the mesopores and macropores increases slowly, and a part of the organic matter begins to pyrolyze to form asphaltenes; at 400−500 °C, the pyrolysis of kerogen leads to the volatilization of a large amount of oil and gas products, the expansion of the pore volume increases, and the volume of the mesopores and macropores increases dramatically.
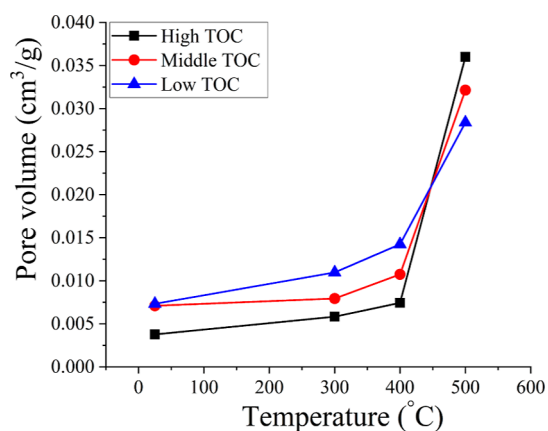
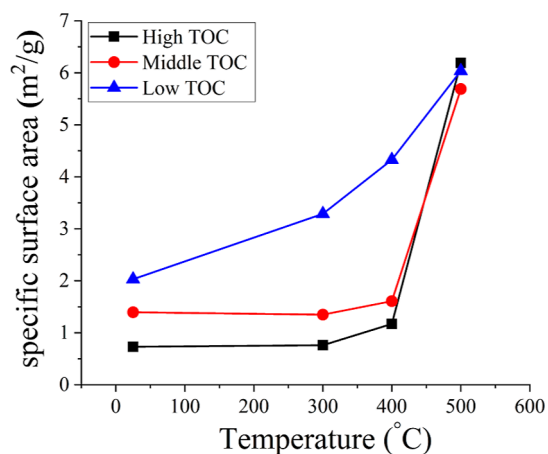**Figure 6.** Relationship between temperature and pore volume change.

Figure 7. Relationship between temperature and surface area.
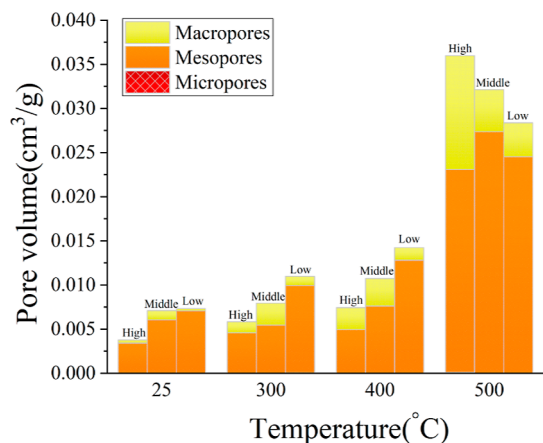

Figure 8. Variation in pore volume in stages under the action of heat.

Figure 9 shows the change in the average pore size of immature shale with high-, medium-, and low-TOC contents at different temperatures. It can be seen from the figure that the average pore size of high- and low-TOC immature shale shows an increase with increasing pyrolysis temperature. The average pore diameter of immature shale increases in the range of 25−400 °C, mainly due to the pyrolysis of organic matter and mineral dehydration; the average pore diameter of high-TOC immature shale increases between 400 and 500 °C is much larger than that of low-TOC immature shale because the
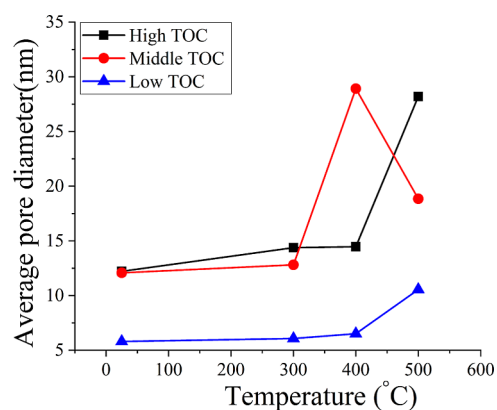

Figure 9. Relationship between temperature and average pore size.

pyrolysis of organic matter is violent in this temperature range, and after the pyrolysis of organic matter, the original micropores interpenetrate and become small pores, so the average pore diameter increases; the higher the organic matter content, the more throughgoing holes form. The average pore size of medium-TOC immature shale increases with the increase in temperature, and the average pore size decreases at 400−500 °C, which may be due to the collapse of the mineral skeleton under the action of high temperature, resulting in a decrease in the number of pores, so the average pore size decreases.

4.1.3. Pore Fractal Characteristics. The relevant parameters of the fractal calculation of immature shale pores in specimens with different TOC contents are shown in Table 3. The fractal dimension reflects the complexity of pores. The change in fractal dimension quantitatively represents the control of the final pyrolysis temperature on the pore evolution of immature shale from a macro perspective. As shown in Figure 10, in the double logarithmic curves of adsorption volume and relative pressure of immature shale from low-temperature liquid nitrogen adsorption tests, the red line shows the linear fitting of the double logarithmic curve of adsorption volume and relative pressure $P/P_0 = 0.5−1$, DFHH reflects the spatial complexity of pores, and the black line shows the linear fitting of the double logarithmic curve of the adsorption volume and relative pressure $P/P_0 = 0−0.5$. The fractal dimension D_S reflects the surface roughness of pores.

Figure 11 shows the variation in the fractal dimension of the pore space of high-, medium-, and low-TOC immature shale with pyrolysis temperature. The correlation factors of the samples are all above 0.9. The fractal dimension has certain geological significance. The fractal dimension of 3 corresponds to the volume filling, and the fractal dimension of 2 corresponds to the smooth surface without pores. According to FHH theory, the calculated D_{FHH} value of high-TOC immature shale is 2.397−2.500, that of medium-TOC immature shale is 2.447−2.503, and that of low-TOC immature shale is 2.519−2.636. It shows that the pore space of the sample is very small, the pore structure is very complex, and the heterogeneity is strong. The D_{FHH} fractal number of high-TOC immature shale first decreases and then increases with temperature. Between 300 and 500 °C, the fractal dimension of medium- and low-TOC immature shale decreases and reaches the minimum value in the whole pyrolysis process, indicating that the internal pore structure of the immature shale at this time uniformly adjusts and becomes simple, which is conducive to the propagation and diffusion of the heat transfer medium in in situ mining. At 300−

Table 3. Immature Shale Fractal Statistics

| | | FHH model | | | | | | | |
| | | P/P_0: 0.5−1 | | | | P/P_0: 0−0.5 | | | |
specimen number	temperature/°C	A	δ	$D = 3 + A$	R^2	A	δ	$D = 3 + A$	R^2
H-1	25	−0.603	−0.809	2.397	0.9902	−0.413	−0.239	2.587	0.9184
H-2	300	−0.536	−0.608	2.464	0.9898	−0.537	−0.611	2.463	0.9455
H-3	400	−0.500	−0.5	2.5	0.9725	−0.597	−0.791	2.403	0.9634
H-4	500	−0.573	−0.719	2.427	0.9902	−0.472	−0.416	2.528	0.9134
M-1	25	−0.497	−0.491	2.503	0.9923	−0.642	−0.926	2.358	0.9768
M-2	300	−0.507	−0.521	2.493	0.9923	−0.637	−0.911	2.363	0.9763
M-3	400	−0.533	−0.599	2.467	0.9679	−0.819	−1.457	2.181	0.9025
M-4	500	−0.553	−0.659	2.447	0.9969	−0.453	−0.359	2.547	0.9799
L-1	25	−0.364	−0.092	2.636	0.9814	−0.596	−0.788	2.404	0.9498
L-2	300	−0.297	0.109	2.703	0.9855	−0.317	0.049	2.683	0.9235
L-3	400	−0.366	−0.098	2.634	0.9866	−0.603	−0.809	2.397	0.9743
L-4	500	−0.481	−0.443	2.519	0.9945	−0.527	−0.581	2.473	0.9867

400 °C, the fractal dimension suddenly increases, indicating that at this stage, the pores increase due to the pyrolysis of organic matter. Small pores dominate, which leads to a complicated pore structure. The fractal number of different TOC immature shale increases with temperature at 400−500 °C. This is because after 400 °C, due to further pyrolysis of organic matter, the pore connectivity improves, and the structure becomes more uniform.

As shown in Figure 12, the fractal dimension Ds of high-, medium-, and low-TOC immature shale varies with the pyrolysis temperature. The fractal dimension Ds reflects the surface roughness of mesopores. With high-TOC immature shale in the range of 25−400 °C, the fractal dimension Ds decreases because, with the increase in temperature, the precipitation of free water and bound water occurs inside the immature shale, and the surface roughness tends to decrease. At 400−500 °C, the fractal dimension Ds of high-TOC immature shale increases because many small pores are generated after the cracking of organic matter at this time, and the roughness increases. The trend of the fractal dimension Ds of medium- and low-TOC immature shale increases first, then decreases, and then increases with temperature. High-, medium-, and low-immature shale have abrupt points at 300−400 °C. This temperature point is also the critical temperature at which organic matter in immature shale begins to decompose, and the temperature action adjusts the particle structure, softens, and deforms the organic matter and begins pyrolysis. Both the pore surface morphology and the spatial structure have produced great changes, resulting in large changes in fractal dimension.

4.2. Analysis of NMR T_2 Distributions. N_2 adsorption/desorption can provide information on only the mesopores of altered samples. For NMR, the samples need not be dried, and thus, pore structural damage can be avoided. There are generally three types of pores in immature shale, namely, organic pores, inorganic pores, and microfractures[55] Sondergeld et al.[56] believe that the short relaxation peak below 3 ms corresponds to the 3−100 nm pores generated by kerogen maturation and hydrocarbon generation.

Figure 13a−c refers to the NMR T_2 spectra of high-, medium-, and low-TOC immature shale at different temperatures, respectively. The NMR T_2 spectra of shale specimens with different TOC contents at room temperature all show a discontinuous bimodal distribution, and a small amount of relaxation signals appear between 100 and 1000 ms, indicating that the immature shale has a small number of microfractures.

When the temperature rises to 300 °C, the NMR T_2 spectrum of the high-TOC immature shale shows a continuous three-peak state. Compared with the results before pyrolysis, the relaxation signal amplitude between 0.01 and 10 ms decreases greatly, and at the same time, there is a relatively high amplitude between 10 and 100 ms. This shows that under the action of heat, not only fine pores but also some relatively large pores and fractures form in the immature shale.[58] The NMR T_2 spectra of the medium- and low-TOC immature shale show a continuous double-peak state, and the amplitude of the relaxation signal decreases between 0.01 and 10 ms. At 400 °C, both the high- and medium-TOC immature shale T_2 spectra show a discontinuous three-peak state. At this time, a large amount of organic matter in the immature shale is pyrolyzed, and the pyrolysis intermediate product asphaltene blocks some pores and reduces the pore continuity. The NMR T_2 spectrum of the low-TOC immature shale exhibits a continuous bimodal state because the immature shale produces less asphaltene so that there is no pore blocking phenomenon. At 500 °C, the NMR T_2 spectrum of high-TOC immature shale evolves into a single peak state. At this time, the asphaltene undergoes secondary cracking, and the pores inside the immature shale have good continuity. The NMR T_2 spectrum of medium-TOC immature shale evolves into a continuous three-peak state, and the connectivity of immature shale improves, while the NMR T_2 spectrum of low-TOC immature shale evolves into a discontinuous double-peak state.[58]

The full pore size distribution of rock samples can be characterized by NMR experiments.[59−62] Many researchers have used the relationship between T_2 time and pore radius, which can be expressed as[42,63−65]

$$\frac{1}{T_2} = \rho \frac{F_S}{r} \tag{5}$$

where r is the pore radius, μm; ρ is the transversal surface relaxivity, μm/ms; F_s is the pore shape factor. For cylindrical and spherical pores, F_S is taken as 2 and 3, respectively.

It is generally believed that the pores in shale are mostly cylindrical, and F_S can take 2.[59,66,67] According to the study of shale surface relaxation rate by Sondergeld et al.,[68] ρ can take 0.05 μm/ms. Thus, eq 5 can be further transformed into
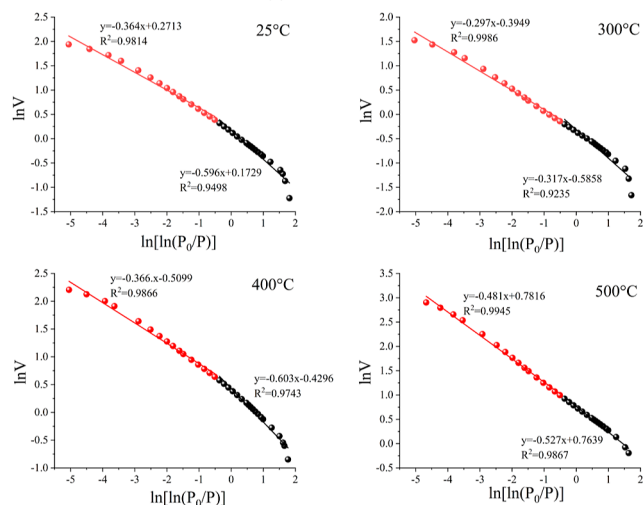
$$r = \frac{T_2}{10} \tag{6}$$
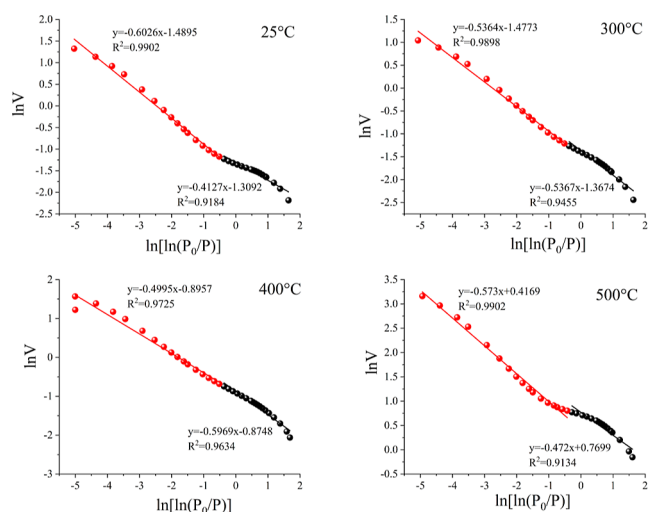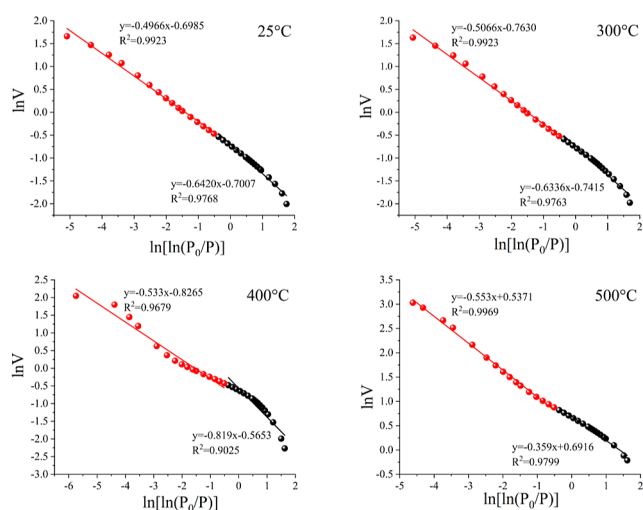
Figure 10. Double logarithmic curves of adsorption volume and relative pressure of immature shale from low-temperature liquid nitrogen adsorption tests.
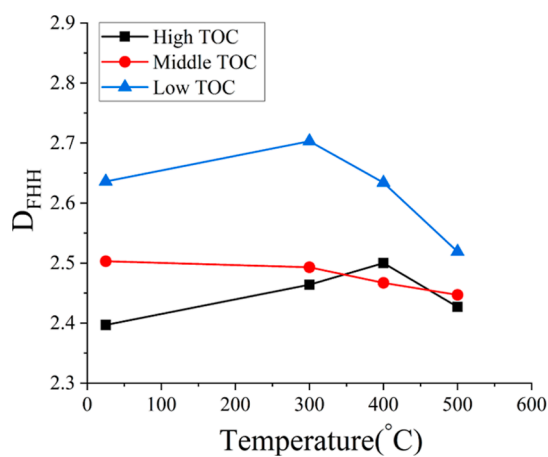

Figure 11. Relationship between fractal dimension of the pore structure and pyrolysis temperature.
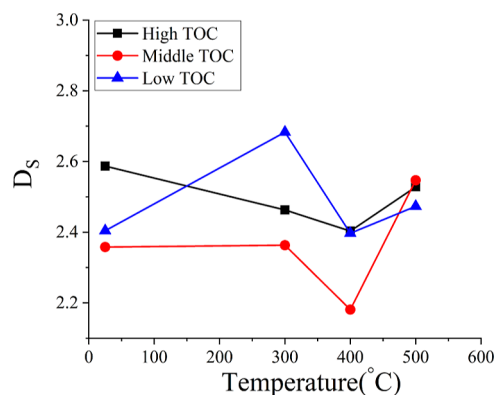

Figure 12. Relationship between fractal dimension of the pore surface and pyrolysis temperature.

samples are mainly distributed in 1−1000 nm, and the peak pore diameter is mainly distributed in 100−130 nm. With the increase of temperature, the peak pore diameter of different TOC immature shale increases. At 300−500 °C, micron level fractures begin to develop, which is likely to be a contraction joint at the edge of organic matter due to hydrocarbon generation shrinkage of organic matter after pyrolysis[57] At 400−500 °C, the peak pore diameter of different TOC immature shale increases sharply. As shown in Figure 15, the pore structure of high-, medium-, and low-TOC immature shale changes greatly at 300−500 °C. The porosity of high-, medium-, and low-TOC immature shale increases by 2.78 times, 1.57 times, and 0.28 times, respectively; during the heating process at 300−500 °C, the organic matter will decompose into asphaltene and dry distillation at 300−400 °C, and the asphaltenes will further decompose into oil, dry distillation gas, and residues at 400−500 °C. The generated oil and gas will volatilize into the air; therefore, the porosity changes greatly, indicating that the organic matter content of immature shale is a major factor affecting the increase in porosity.

4.3. Comparison of Results from LTNA and NMR. This study investigated the pore structure from 2 nm to 1000 μm, and the results comprehensively described the evolution of the pore structure of immature shale with different organic matter. The LNTA method can effectively characterize the pore structure characteristics of immature shale with pore sizes of 2−300 nm, and the NMR method can truly reflect the pore size distribution
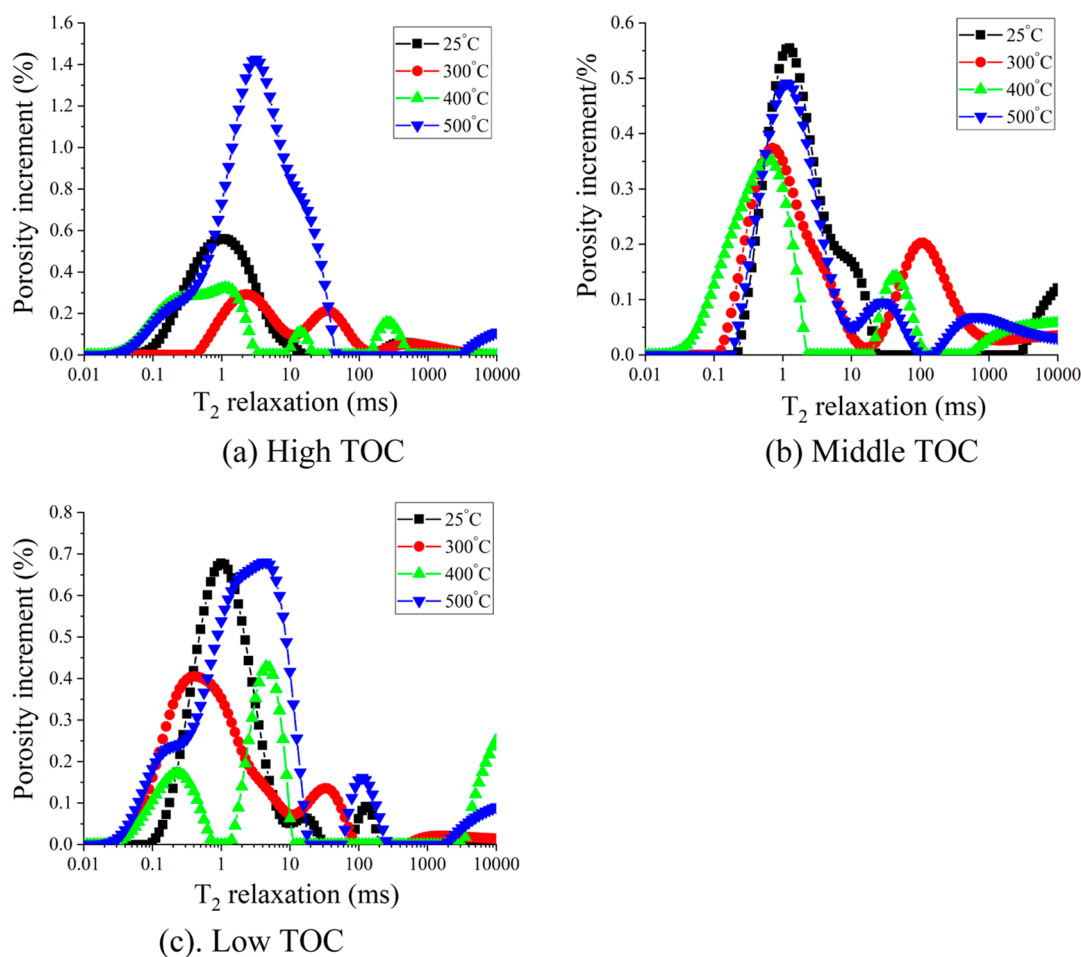
To clearly characterize PSD, NMR spectrum was transformed via eq 6, As illustrated in Figure 14, the pore diameter of the

(a) High TOC

(b) Middle TOC

(c). Low TOC

Figure 13. NMR T_2 spectra of immature shale after pyrolysis at different temperatures.

evolution of immature shale samples, especially macropores and cracks.[66,69] At 500 °C, the porosity of high-TOC immature shale, measured by the NMR test, reaches its maximum value, so do the pore volume and pore diameter measured by LTNA; this phenomenon shows that the pyrolysis of organic matter greatly influences the pore structure of immature shale during the heating process. According to the NMR test, at 300−500 °C, microcracks begin to develop, and the LTNA experiment cannot observe pores of this scale. At 400−500 °C, the peak pore diameter of different TOC immature shale increases sharply, which is consistent with the law of LTNA.

4.4. Evolution Mechanism of the Pore Structure of Immature Shale. The evolution of the immature shale pore structure is essentially the result of the physical and chemical reactions of the organic kerogen and inorganic matter in the immature shale under the action of heat, and the change in temperature causes the rearrangement of the immature shale pore structure. At 25−300 °C, the effect of temperature removes the free water in the pores of the immature shale and at the same time causes the inorganic minerals to be finely adjusted under the action of thermal stress. Due to the strong sensitivity of clay minerals to water, water molecules may occupy the adsorption position in mesopores and block the pore throat through dispersed or dissolved clay minerals; therefore, the volume of the mesopore increases from 25 to 300 °C.[70,71] This process has relatively little effect on the pore structure, and the volume and specific surface area of the small pores increase slightly. At 300−400 °C, the kerogen begins to transform into polymer insoluble

matter at a certain temperature, and the linear polymer-insoluble matter is decomposed into asphaltene and dry distillation gas at high temperature.[72] A large amount of organic matter in the immature shale is pyrolyzed to form pore space, and the pressure of gas products also plays a role of "expanding"; therefore, the small pore volume of shale specimens with different TOC contents increases significantly at this time. At 400−500 °C, as the temperature continued to rise, the asphaltenes further decomposed into oil, and dry distillation gas and residues were generated. Immature shale with a higher organic matter content has a greater hydrocarbon expulsion strength and a higher pore volume growth rate. In addition, thermal stress leads to the fracture of the inorganic mineral framework to form pores and fissures. Under the action of multiple factors, the shape and structure of pores change significantly, and the structure of pores becomes more developed and complex. The internal pressure of solid particles increases with increasing pyrolysis temperature. The pressure inside the solid particles increases with increasing pyrolysis temperature, which causes the rapid eruption of a large amount of shale oil and gas, resulting in the opening of pores, micropores, and small holes and an increased number of large holes. At the same time, adjacent pores become interconnected, resulting in an increase in the immature shale porosity. Therefore, studying the evolution of the pore structure of shale specimens with different TOC contents before and after pyrolysis can provide an engineering reference for the in situ exploitation of immature shale in different horizons of the same reservoir.
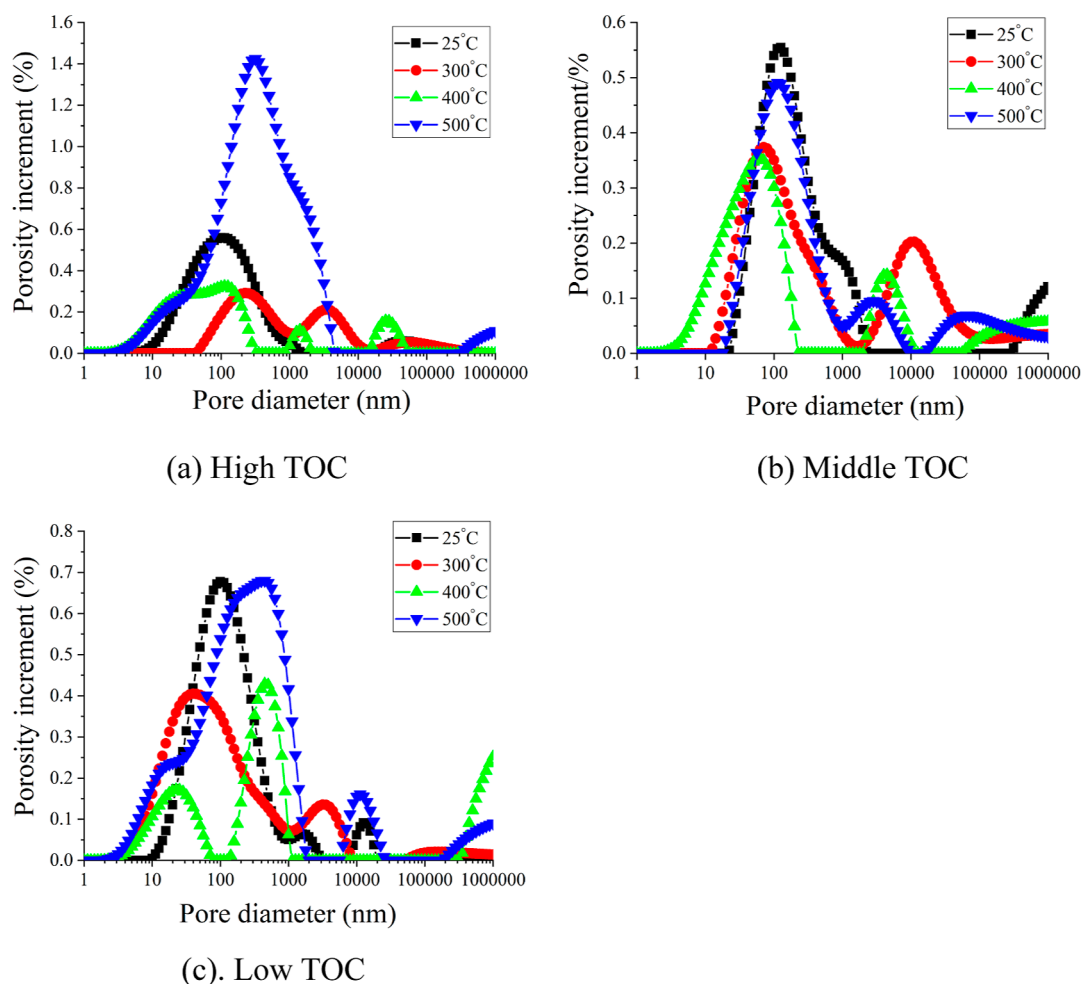
(a) High TOC

(b) Middle TOC

(c). Low TOC

Figure 14. Pore size distribution of immature shale that are converted from NMR T_2 distribution after pyrolysis at different temperatures.
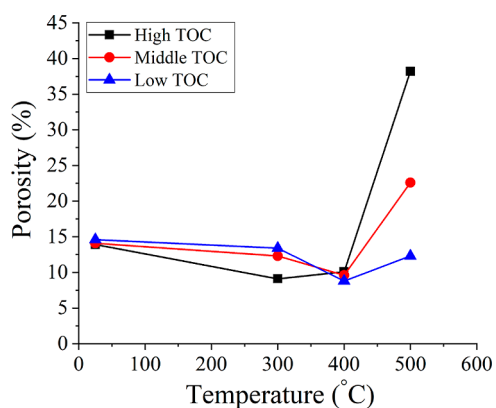

Figure 15. Variation in porosity in shale specimens with different TOC contents with different temperatures.

5. CONCLUSIONS

In this paper, immature shale is heated and pyrolyzed in a tube furnace, and the pore structure evolution of the shale specimens with different TOC contents under different temperature conditions is studied by comprehensive use of NMR tests and low-temperature liquid nitrogen tests. The following main conclusions are obtained:

(1) The adsorption branches of nitrogen absorption–desorption isotherms in different TOC immature shale after pyrolysis at high temperature can be divided into three stages. The pore structure of different TOC immature shale is all slit-shaped after pyrolysis at different temperatures.

(2) Before 400 °C, organic matter cracking will form asphaltene, and asphaltene will block part of the pores, and at 500 °C, the blocked pores will be dredged because of the secondary cracking of asphaltene; the higher the organic matter content of the immature shale under high temperatures, the greater the change in pore volume and specific surface area.

(3) The pores of the shale in the study area have significant fractal characteristics, the correlation factor of the FHH model is above 0.9, the fractal dimension is between 2.397-2.636, the pore space of the sample is extremely small, the pore structure is extremely complex, and the heterogeneity is strong. The temperature effect makes the particle structure develop and adjust, softens and deforms the organic matter, and begins pyrolysis; both the pore surface morphology and the spatial structure produce great changes, resulting in a large change in the fractal dimension.

(4) During the heating process of high-TOC immature shale at 300−500 °C, the porosity increases with increasing temperature, while the porosity of medium- and low-TOC immature shale increases with increasing temperature, with a slight decrease followed by a rapid increase. The porosity of high-, medium-, and low-TOC immature shale increases during the heating process of 400−500 °C, indicating that there is a critical point within this range.

■ AUTHOR INFORMATION

Corresponding Author

Lingzhi Xie − *State Key Laboratory of Hydraulic and Mountain River Engineering, College of Architecture and Environment, Sichuan University, Chengdu 610065, China; Department of Civil Engineering, College of Architecture and Environment and Institute of New Energy and Low-Carbon Technology, Sichuan University, Chengdu 610065, China;*
Email: xielingzhi@scu.edu.cn

Authors

Luo Zhuoke − *State Key Laboratory of Hydraulic and Mountain River Engineering, College of Architecture and Environment, Sichuan University, Chengdu 610065, China; Department of Civil Engineering, College of Architecture and Environment, Sichuan University, Chengdu 610065, China;* orcid.org/0000-0002-3839-0812

Tiefeng Lin − *Exploration and Development Research Institute of Daqing Oilfield Co Ltd., Daqing 163712, China; Heilongjiang Key Laboratory of Tight Oil and Shale Oil Accumulations, Daqing 163712, China*

Xin Liu − *Exploration and Development Research Institute of Daqing Oilfield Co Ltd., Daqing 163712, China; Heilongjiang Key Laboratory of Tight Oil and Shale Oil Accumulations, Daqing 163712, China*

Shengming Ma − *Exploration and Development Research Institute of Daqing Oilfield Co Ltd., Daqing 163712, China; Heilongjiang Key Laboratory of Tight Oil and Shale Oil Accumulations, Daqing 163712, China*

Xin Li − *Exploration and Development Research Institute of Daqing Oilfield Co Ltd., Daqing 163712, China; Heilongjiang Key Laboratory of Tight Oil and Shale Oil Accumulations, Daqing 163712, China*

Fan Yang − *Exploration and Development Research Institute of Daqing Oilfield Co Ltd., Daqing 163712, China; Heilongjiang Key Laboratory of Tight Oil and Shale Oil Accumulations, Daqing 163712, China*

Bo He − *Institute of New Energy and Low-Carbon Technology, Sichuan University, Chengdu 610065, China*

Jun Liu − *Institute of New Energy and Low-Carbon Technology, Sichuan University, Chengdu 610065, China*

Yao Zhang − *State Key Laboratory of Hydraulic and Mountain River Engineering, College of Architecture and Environment, Sichuan University, Chengdu 610065, China; Department of Civil Engineering, College of Architecture and Environment, Sichuan University, Chengdu 610065, China*

Complete contact information is available at:
https://pubs.acs.org/10.1021/acsomega.2c07990

Notes
The authors declare no competing financial interest.

■ REFERENCES

(1) Selin, R. *The Outlook for Energy: A View to 2040*; ExxonMobil, 2013; pp 1−14.

(2) Khatib, H. IEA world energy outlook 2010–A comment. *Energy Pol.* **2011**, *39*, 2507−2511.

(3) Dyni, J. R. Geology and resources of some world oil-shale deposits. *Oil Shale* **2003**, *20*, 193−252.

(4) Fletcher, T. H.; Gillis, R.; Adams, J.; Hall, T.; Mayne, C. L.; Solum, M. S.; Pugmire, R. J. Characterization of macromolecular structure elements from a Green River oil shale, II. Characterization of pyrolysis products by 13C NMR, GC/MS, and FTIR. *Energy Fuels* **2014**, *28*, 2959−2970.

(5) Sun, Y.; Bai, F.; Liu, B.; Liu, Y.; Guo, M.; Guo, W.; Wang, Q.; Lü, X.; Yang, F.; Yang, Y. Characterization of the oil shale products derived via topochemical reaction method. *Fuel* **2014**, *115*, 338−346.

(6) Trikkel, A.; Kuusik, R.; Martins, A.; Pihu, T.; Stencel, J. M. Utilization of Estonian oil shale semicoke. *Fuel Process. Technol.* **2008**, *89*, 756−763.

(7) Pan, Y.; Zhang, X.; Liu, S.; Yang, S.; Ren, N. A review on technologies for oil shale surface retort. *J. Chem. Soc. Pak.* **2012**, *34*, 1331−1338.

(8) Gavrilova, O.; Vilu, R.; Vallner, L. A life cycle environmental impact assessment of oil shale produced and consumed in Estonia. *Resour. Conserv. Recycl.* **2010**, *55*, 232−245.

(9) Velts, O.; Uibu, M.; Rudjak, I.; Kallas, J.; Kuusik, R. Utilization of oil shale ash to prepare PCC: Leachability dynamics and equilibrium in the ash-water system. *Energy Proc.* **2009**, *1*, 4843−4850.

(10) Shi, M.; Yu, B.; Zhang, J.; Huang, H.; Yuan, Y.; Li, B. Evolution of organic pores in marine shales undergoing thermocompression: A simulation experiment using hydrocarbon generation and expulsion. *J. Nat. Gas Sci. Eng.* **2018**, *59*, 406−413.

(11) Xu, H.; Yu, H.; Fan, J.; Xia, J.; Liu, H.; Wu, H. Formation mechanism and structural characteristic of pore-networks in shale kerogen during in-situ conversion process. *Energy* **2022**, *242*, 122992.

(12) Wang, L.; Yang, D.; Kang, Z.; Zhao, J.; Meng, Q. Experimental study on the effects of steam temperature on the pore-fracture evolution of oil shale exposed to the convection heating. *J. Anal. Appl. Pyrolysis* **2022**, *164*, 105533.

(13) Perez, F.; Devegowda, D. A molecular dynamics study of primary production from shale organic pores. *SPE J.* **2020**, *25*, 2521−2533.

(14) Gou, Q.; Xu, S.; Hao, F.; Yang, F.; Shu, Z.; Liu, R. The effect of tectonic deformation and preservation condition on the shale pore structure using adsorption-based textural quantification and 3D image observation. *Energy* **2021**, *219*, 119579.

(15) Aljaberi, J.; Alafnan, S.; Glatz, G.; Sultan, A. S.; Afagwu, C. The impact of kerogen tortuosity on shale permeability. *SPE J.* **2021**, *26*, 765−779.

(16) Duvall, F.; Sohn, Y. S.; Pitt, C. H. Physical behaviour of oil shale at various temperatures and compressive loads: 3. Structural failure under loads. *Fuel* **1985**, *64*, 938−940.

(17) Kang, Z. Q.; Yang, D.; Zhao, Y. S.; Hu, Y. Q. Thermal Cracking and Corresponding Permeability of Fushun Oil Shale. *Oil Shale* **2011**, *28*, 273−283.

(18) Tiwari, P.; Deo, M.; Lin, C. L.; Miller, J. D. Characterization of oil shale pore structure before and after pyrolysis by using X-ray micro CT. *Fuel* **2013**, *107*, 547−554.

(19) Rabbani, A.; Baychev, T. G.; Ayatollahi, S.; Jivkov, A. P. Evolution of pore-scale morphology of oil shale during pyrolysis: a quantitative analysis. *Transp. Porous Media* **2017**, *119*, 143−162.

(20) Saif, T.; Lin, Q.; Butcher, A. R.; Bijeljic, B.; Blunt, M. J. Multi-scale multi-dimensional microstructure imaging of oil shale pyrolysis using X-ray micro-tomography, automated ultra-high resolution SEM, MAPS Mineralogy and FIB-SEM. *Appl. Energy* **2017**, *202*, 628−647.

(21) Sun, L.; Tuo, J.; Zhang, M.; Wu, C.; Wang, Z.; Zheng, Y. Formation and development of the pore structure in Chang 7 member oil-shale from Ordos Basin during organic matter evolution induced by hydrous pyrolysis. *Fuel* **2015**, *158*, 549−557.

(22) Han, X.; Jiang, X.; Cui, Z. Change of pore structure of oil shale particles during combustion. 2. Pore structure of oil-shale ash. *Energy Fuels* **2008**, *22*, 972−975.

(23) Yang, L.; Yang, D.; Zhao, J.; Liu, Z.; Kang, Z. Changes of oil shale pore structure and permeability at different temperatures. *Oil Shale* **2016**, *33*, 101.

(24) Bai, F.; Sun, Y.; Liu, Y.; Guo, M. Evaluation of the porous structure of Huadian oil shale during pyrolysis using multiple approaches. *Fuel* **2017**, *187*, 1−8.

(25) Geng, Y.; Liang, W.; Liu, J.; Cao, M.; Kang, Z. Evolution of pore and fracture structure of oil shale under high temperature and high pressure. *Energy Fuels* **2017**, *31*, 10404−10413.

(26) Tisot, P. R. Alterations in structure and physical properties of Green River oil shale by thermal treatment. *J. Chem. Eng. Data* **1967**, *12*, 405−411.

(27) Kobchenko, M.; Panahi, H.; Renard, F.; Dysthe, D. K.; Malthe-Sørenssen, A.; Mazzini, A.; Scheibert, J.; Jamtveit, B.; Meakin, P. 4D imaging of fracturing in organic-rich shales during heating. *J. Geophys. Res.: Solid Earth* **2011**, *116*, B12201.

(28) Feng, Z.-q.; Jia, C.-z.; Xie, X.; Zhang, S.; Feng, Z.; Cross, T. A. Tectonostratigraphic units and stratigraphic sequences of the nonmarine Songliao basin, northeast China. *Basin Res.* **2010**, *22*, 79−95.

(29) Yang, W.; Yongkang, L.; Ruiqi, G. Formation and evolution of nonmarine petroleum in Songliao Basin, China. *AAPG Bull.* **1985**, *69*, 1112−1122.

(30) Wan, X.; Zhao, J.; Scott, R. W.; Wang, P.; Feng, Z.; Huang, Q.; Xi, D. Late Cretaceous stratigraphy, Songliao Basin, NE China: SK1 cores. *Palaeogeogr., Palaeoclimatol., Palaeoecol.* **2013**, *385*, 31−43.

(31) Cao, H.; He, W.; Chen, F.; Kong, D. Superheavy pyrite in the Upper Cretaceous mudstone of the Songliao Basin, NE China and its implication for paleolimnological environments. *J. Asian Earth Sci.* **2020**, *189*, 104156.

(32) He, W.; Sun, Y.; Guo, W.; Shan, X.; Su, S.; Zheng, S.; Deng, S.; Kang, S.; Zhang, X. Organic geochemical characteristics of the upper Cretaceous Qingshankou Formation oil shales in the Fuyu oilfield, Songliao Basin, China: Implications for oil-generation potential and depositional environment. *Energies* **2019**, *12*, 4778.

(33) Li, T.; Huang, Z.; Zhao, J.; Xu, X.; Guo, X. Pore structure characteristics and their influencing factors: a case study from the middle jurassic mixed siliciclastic carbonate rocks, Turpan-Hami basin, Northwest China. *J. Petrol. Sci. Eng.* **2021**, *203*, 108611.

(34) Brunauer, S.; Emmett, P. H.; Teller, P. Adsorption of gases in multimolecular layers. *J. Am. Chem. Soc.* **1938**, *60*, 309−319.

(35) Barrett, E. P.; Joyner, L. G.; Halenda, P. P. The determination of pore volume and area distributions in porous substances. I. Computations from nitrogen isotherms. *J. Am. Chem. Soc.* **1951**, *73*, 373−380.

(36) Liu, Z.; Liu, D.; Cai, Y.; Yao, Y.; Pan, Z.; Zhou, Y. Application of nuclear magnetic resonance (NMR) in coalbed methane and shale reservoirs: A review. *Int. J. Coal Geol.* **2020**, *218*, 103261.

(37) Pfeifer, P.; Obert, M.; Cole, M. Fractal BET and FHH theories of adsorption: a comparative study. *Proc. R. Soc. London, Ser. A* **1989**, *423*, 169−188.

(38) Neimark, A. V.; Unger, K. K. Method of discrimination of surface fractality. *J. Colloid Interface Sci.* **1993**, *158*, 412−419.

(39) Pfeifer, P.; Avnir, D. Chemistry in noninteger dimensions between two and three. I. Fractal theory of heterogeneous surfaces. *J. Chem. Phys.* **1983**, *79*, 3558−3565.

(40) Ismail, I.; Pfeifer, P. Fractal Analysis and Surface Roughness of Nonporous Carbon Fibers and Carbon Blacks. *Langmuir* **1994**, *10*, 1532−1538.

(41) Yao, Y.; Liu, D.; Tang, D.; Tang, S.; Huang, W. Fractal characterization of adsorption-pores of coals from North China: an investigation on CH4 adsorption capacity of coals. *Int. J. Coal Geol.* **2008**, *73*, 27−42.

(42) Li, Z.; Shen, X.; Qi, Z.; Hu, R. Study on the pore structure and fractal characteristics of marine and continental shale based on mercury porosimetry, N2 adsorption and NMR methods. *J. Nat. Gas Sci. Eng.* **2018**, *53*, 12−21.

(43) Yuan, Y.; Rezaee, R. Fractal analysis of the pore structure for clay bound water and potential gas storage in shales based on NMR and N2 gas adsorption. *J. Petrol. Sci. Eng.* **2019**, *177*, 756−765.

(44) Kuila, U.; Prasad, M. Specific surface area and pore-size distribution in clays and shales. *Geophys. Prospect.* **2013**, *61*, 341−362.

(45) Külaots, I.; Goldfarb, J. L.; Suuberg, E. M. Characterization of Chinese, American and Estonian oil shale semicokes and their sorptive potential. *Fuel* **2010**, *89*, 3300−3306.

(46) Xi, Z.; Tang, S.; Zhang, S.; Sun, K. Pore structure characteristics of marine−continental transitional shale: A case study in the Qinshui Basin, China. *Energy Fuels* **2017**, *31*, 7854−7866.

(47) Budaeva, A. D.; Zoltoev, E. V. Porous structure and sorption properties of nitrogen-containing activated carbon. *Fuel* **2010**, *89*, 2623−2627.

(48) Sing, K. S. Reporting physisorption data for gas/solid systems with special reference to the determination of surface area and porosity (Recommendations 1984). *Pure Appl. Chem.* **1985**, *57*, 603−619.

(49) Rouquerol, J.; Avnir, D.; Fairbridge, C.; Everett, D.; Haynes, J.; Pernicone, N.; Ramsay, J.; Sing, K.; Unger, K. Recommendations for the characterization of porous solids (Technical Report). *Pure Appl. Chem.* **1994**, *66*, 1739−1758.

(50) Korost, D. V.; Nadezhkin, D. V.; Akhmanov, G. G. Pore space in source rock during the generation of hydrocarbons. *Moscow Univ. Geol. Bull.* **2012**, *67*, 240−246.

(51) Liu, D.; Li, H.; Zhang, C.; Wang, Q.; Peng, P. a. Experimental investigation of pore development of the Chang 7 member shale in the Ordos basin under semi-closed high-pressure pyrolysis. *Mar. Pet. Geol.* **2019**, *99*, 17−26.

(52) Chandra, D.; Bakshi, T.; Bahadur, J.; Hazra, B.; Vishal, V.; Kumar, S.; Sen, D.; Singh, T. Pore morphology in thermally-treated shales and its implication on CO2 storage applications: A gas sorption, SEM, and small-angle scattering study. *Fuel* **2023**, *331*, 125877.

(53) Tan, J.; Hu, R.; Luo, W.; Ma, Z.; He, G. Pore evolution of lacustrine organic-rich shales: insights from thermal simulation experiments. *Energy Fuels* **2021**, *35*, 3079−3094.

(54) Wang, X.; Wang, M.; Li, J.; Shao, H.; Deng, Z.; Wu, Y. Thermal maturity: The controlling factor of wettability, pore structure, and oil content in the lacustrine Qingshankou shale, Songliao Basin. *J. Petrol. Sci. Eng.* **2022**, *215*, 110618.

(55) Loucks, R. G.; Reed, R. M.; Ruppel, S. C.; Hammes, U. Spectrum of pore types and networks in mudrocks and a descriptive classification for matrix-related mudrock pores. *AAPG Bull.* **2012**, *96*, 1071−1098.

(56) Curtis, M. E.; Cardott, B. J.; Sondergeld, C. H.; Rai, C. S. Development of organic porosity in the Woodford Shale with increasing thermal maturity. *Int. J. Coal Geol.* **2012**, *103*, 26−31.

(57) Li, G.; Ma, Z.; Zheng, J.; Bao, F.; Zheng, L. NMR analysis of the physical change of oil shales during in situ pyrolysis at different temperatures. *Pet. Geol. Exp.* **2016**, *38*, 402−406.

(58) Gao, H.; Wang, C.; Cao, J.; He, M.; Dou, L. Quantitative study on the stress sensitivity of pores in tight sandstone reservoirs of Ordos basin using NMR technique. *J. Petrol. Sci. Eng.* **2019**, *172*, 401−410.

(59) Li, A.; Ding, W.; Wang, R.; He, J.; Wang, X.; Sun, Y.; Gu, Y.; Jiao, N. Petrophysical characterization of shale reservoir based on nuclear magnetic resonance (NMR) experiment: A case study of Lower Cambrian Qiongzhusi Formation in eastern Yunnan Province, South China. *J. Nat. Gas Sci. Eng.* **2017**, *37*, 29−38.

(60) Liu, Y.; Yao, Y.; Liu, D.; Zheng, S.; Sun, G.; Chang, Y. Shale pore size classification: An NMR fluid typing method. *Mar. Pet. Geol.* **2018**, *96*, 591−601.

(61) Chen, Y.; Jiang, C.; Leung, J. Y.; Wojtanowicz, A. K.; Zhang, D. Multiscale characterization of shale pore-fracture system: Geological controls on gas transport and pore size classification in shale reservoirs. *J. Petrol. Sci. Eng.* **2021**, *202*, 108442.

(62) Wang, J.; Zhang, Q.; Song, Z.; Liu, X.; Wang, X.; Zhang, Y. Microstructural variations and damage evolvement of salt rock under cyclic loading. *Int. J. Rock Mech. Min. Sci.* **2022**, *152*, 105078.

(63) Coates, G. R. NMR logging principles and applications; Halliburton Energy Services, 1999.

(64) Zhao, P.; He, B.; Zhang, B.; Liu, J. Porosity of gas shale: Is the NMR-based measurement reliable? *Pet. Sci.* **2022**, *19*, 509−517.

(65) Wang, L.; Zhao, N.; Sima, L.; Meng, F.; Guo, Y. Pore structure characterization of the tight reservoir: systematic integration of mercury

injection and nuclear magnetic resonance. *Energy Fuels* **2018**, *32*, 7471−7484.

(66) Zhao, P.; Wang, X.; Cai, J.; Luo, M.; Zhang, J.; Liu, Y.; Rabiei, M.; Li, C. Multifractal analysis of pore structure of Middle Bakken formation using low temperature N2 adsorption and NMR measurements. *J. Petrol. Sci. Eng.* **2019**, *176*, 312−320.

(67) Zhao, R.; Xue, H.; Lu, S.; Li, J.; Tian, S.; wang, Z.; Dong, Z. Multi-scale pore structure characterization of lacustrine shale and its coupling relationship with material composition: An integrated study of multiple experiments. *Mar. Pet. Geol.* **2022**, *140*, 105648.

(68) Sondergeld, C. H.; Ambrose, R. J.; Rai, C. S.; Moncrieff, J. Micro-structural studies of gas shales. In *SPE unconventional gas conference*; OnePetro, 2010, p 131771.

(69) Zhou, L.; Kang, Z. Fractal characterization of pores in shales using NMR: A case study from the Lower Cambrian Niutitang Formation in the Middle Yangtze Platform, Southwest China. *J. Nat. Gas Sci. Eng.* **2016**, *35*, 860−872.

(70) Ju, Y.; Hongling, B.; Guochang, W. Main characteristics of shale gas reservoir and its effect on the reservoir reconstruction. *Adv. Earth Sci.* **2014**, *29*, 492−506.

(71) Gu, Y.; Li, X.; Yang, S.; Wan, Q. Microstructure Evolution of Organic Matter and Clay Minerals in Shales with Increasing Thermal Maturity. *Acta Geol. Sin.* **2020**, *94*, 280−289.

(72) Ramos-Fernandez, M.; Normand, L.; Sorbier, L. Structural and morphological characterization of alumina supported Pd nanoparticles obtained by colloidal synthesis. *Oil Gas Sci. Technol.* **2007**, *62*, 101−113.